Journal of Materials Chemistry

Cite this: *J. Mater. Chem.*, 2012, **22**, 4704

www.rsc.org/materials

PAPER

Direct synthesis of dextran-coated superparamagnetic iron oxide nanoparticles in a capillary-based droplet reactor†

Kritika Kumar,‡[a] Adrian M. Nightingale,‡[a] Siva H. Krishnadasan,[a] Nazila Kamaly,[a] Marzena Wylenzinska-Arridge,[a] Katharina Zeissler,[a] Will R. Branford,[a] Ecaterina Ware,[a] Andrew J. deMello*[b] and John C. deMello*[a]

Received 13th January 2012, Accepted 20th January 2012
DOI: 10.1039/c2jm30257h

We describe the controlled synthesis of dextran-coated superparamagnetic iron oxide nanoparticles (SPIONs) using a stable passively-driven capillary-based droplet reactor. High quality highly crystalline particles were obtained with a narrow size distribution of mean diameter 3.6 nm and standard deviation 0.8 nm. The particles were evaluated for use in MRI, and found to exhibit a large saturation magnetisation of 58 emu/g and a high T_2 relaxivity of 66 $mM^{-1}s^{-1}$ at 4.7 T, signifying good MRI contrast enhancement properties.

Introduction

Superparamagnetic iron oxide nanoparticles (SPIONs) are of significant interest due to wide-ranging applications in areas such as drug delivery,[1] hyperthermic treatment,[2] magnetic resonance imaging (MRI)[3] and selective separation of biological fluids.[4] For all these applications there is a recognised need for improved synthetic methods that are capable of yielding high quality SPIONs of uniform size, geometry and stoichiometry.

In 2002 Edel *et al.*[5] proposed the use of microfluidic reactors for nanoparticle synthesis due to the high levels of control they provide over key reaction parameters such as temperature, reagent concentrations and reaction time. Since that report a diversity of metal,[6] metal oxide,[7] compound semiconductor[8] and organic nanomaterials[9] have been successfully synthesised in microfluidic systems, and in virtually all cases clear advantages were demonstrated over traditional bulk methods in terms of improved reaction yields, size distributions, and shape control.[10]

Most reports of nanoparticle synthesis in microreactors have involved a continuous flow (single-phase) mode of operation, in which continuous (laminar) streams of miscible fluids are manoeuvred through microscale channels where nucleation and growth take place. Continuous flow reactors, however, are poorly suited to the synthesis of rapidly formed nanoparticles such as metal oxides due to their high susceptibility to fouling.[7a,7c] An alternative approach is to use droplet-based reactors in which an immiscible liquid is injected alongside the reaction mixture, causing the latter to spontaneously divide into a series of near identical droplets.[11,12] The immiscible phase is selected so as to preferentially wet the channel surface and hence keep the reacting species away from the walls, drastically reducing the risk of fouling (note, droplet flow also ensures the reagent mixture is carried through the channel at a constant linear velocity, and so beneficially eliminates velocity dispersion which can be a significant cause of polydispersity in laminar flow reactors).[13]

To date there have been very few reports of iron oxide synthesis in microfluidic reactors,[7a,c,14] of which only one by Frenz and co-workers has utilised droplet flow. Using a poly(dimethylsiloxane) microchip with surface-modified channels and micro-fabricated electrodes, they synthesised uncoated SPIONs by merging separate droplets of $Fe(II)Cl_2$/$Fe(III)Cl_3$ and NH_4OH under the influence of a 200 V applied AC voltage. Although this methodology was shown to provide highly synchronised droplet fusion with a low rate of pairing errors and minimal fouling of the reactor, very few details were provided about the quality of the resultant particles. In this manuscript we report a simpler *passive* methodology for preparing dextran-coated SPIONs in droplets, and evaluate the suitability of the particles for use as MRI contrast agents. Compared to the method of Frenz *et al.*, the capillary-based approach we employ obviates the need for lithographic fabrication steps, requires no surface modification of the channel walls, and eliminates the need for high voltage power sources, yet still provides good product quality and high materials throughput. Importantly, the method we report overcomes many of the usual limitations associated with the co-precipitation method,[15] allowing for the straightforward aqueous production of low polydispersity SPIONs with high saturation magnetisations and good MRI contrast enhancement properties.

[a]*Imperial College London, Exhibition Road, South Kensington, London SW72AZ, UK. E-mail: j.demello@imperial.ac.uk*
[b]*Dept. Chemistry & Applied Biosciences, ETH Zurich, HCI F 117, Wolfgang-Pauli-Strasse 10, CH-8093 Zurich, Switzerland. E-mail: andrew.demello@chem.ethz.ch*

† Electronic supplementary information (ESI) available: A video of the capillary reactor in operation, and a figure comparing its operation in droplet- and continuous-flow modes. See DOI: 10.1039/c2jm30257h

‡ These authors contributed equally to the work.

Results and discussion

Fig. 1 illustrates the operation of the droplet reactor (see ref. 12 and Experimental for further details). Droplets are formed close to the end of a length of silicone tubing (1 mm i.d.) at the contact point between two auxiliary capillaries. The capillaries pierce the tubing from opposing sides and meet at an angle of 90° at the capillary centre, with the silicone forming a tight leak-proof seal around them. Two separate syringe pumps (PHD 2000, Harvard Instruments) feed the auxiliary capillaries with aqueous reagents, and a third syringe pump maintains a constant flow of immiscible octadecene carrier fluid through the main capillary. A bead of the merged reagent streams forms at the confluence of the auxiliary capillaries and – under the combined influence of radial forces due to surface tension and axial forces due to viscous drag from the carrier fluid – adopts an ovoid geometry. As the bead grows, it thins at the meeting point and eventually buds-off as a discrete droplet that is carried downstream into a polytetrafluoroethylene (PTFE) capillary (0.82 mm i.d.). The reagents mix inside the droplet as they are motivated along the PTFE capillary by the carrier fluid. (A video recording of the device in operation is provided in the ESI).

For the syntheses reported here, a precursor solution comprising 0.02 M $FeCl_2 \cdot 4H_2O$ (99%, Sigma Aldrich UK), 0.04 M $FeCl_3 \cdot 6H_2O$ (97%, Sigma Aldrich UK) and 0.05 M dextran (MW 10 000, Sigma Aldrich UK) all dissolved in 0.4 M hydrochloric acid (Sigma Aldrich, UK) was injected into one auxiliary capillary at 133 μl min^{-1}; and aqueous NH_4OH (28% NH_3 in H_2O, Sigma Aldrich) was injected into the other capillary at 67 μl min^{-1}. The flow-rate of the carrier fluid was fixed at 600 μl min^{-1}. The rapid increase in pH (from 4 to 11) experienced by the $FeCl_3/FeCl_2$ precursor solution on addition of the NH_4OH induces alkaline co-precipitation of particulate iron oxide,[16] with the dextran co-ordinating to the surface of the particles and stabilising them in the nm size regime. The use of dextran as a surfactant also ensures a high level of biocompatibility,[17] enabling the as-produced particles to be used directly for biological applications without further surface functionalisation.

Brown particles of iron oxide were observed to form inside the droplets immediately after the confluence of the reagent streams (see ESI). From here, the droplets were carried downstream at 1.7 cm s^{-1} into a 4 m section of capillary, immersed in a 60 °C oil bath to aid particle growth and crystallisation.[18,19] Importantly the growing particles remained fully compartmentalised within the droplets as they passed along the length of capillary and showed no tendency to coat the channel walls. In contrast, when the carrier flow was stopped and the reaction was allowed to proceed in a continuous flow (single-phase) mode of operation, a dark brown deposit formed on the inner surface of the main channel within minutes. (Note, a photographic comparison of the two modes of operation is provided in ESI† figure S1). For the droplet-based experiments, the effluent was collected at the capillary outlet over a period of three hours, after which the organic carrier phase was removed and the remaining aqueous solution containing the iron oxide nanoparticles was purified (see Experimental). For comparison, non-coated particles were also synthesised in droplet-flow by omitting the dextran from the iron precursor solution.

Fig. 2a shows a typical Transmission Electron Micrograph (TEM) of the droplet-synthesised particles. The purified particles were isotropic in shape, having a narrow log-normal size distribution of mean diameter $d = 3.6$ nm and standard deviation $\sigma_d = 0.8$ nm (see Fig. 2b). Energy Dispersive X-Ray (EDX) spectroscopy confirmed the presence of iron oxide (data not shown), and Selected Area Electron Diffraction (SAED) measurements (Fig. 2c) showed the particles to be crystalline. The discrete diffraction lines obtained from the SAED were in close correspondence with the inter-planar distances of the spinel phases of iron oxide, Fe_3O_4 and γ-Fe_2O_3,[20] both of which exhibit superparamagnetism at the nanoscale and have similar magnetic properties.[15] No other diffraction lines were observed,

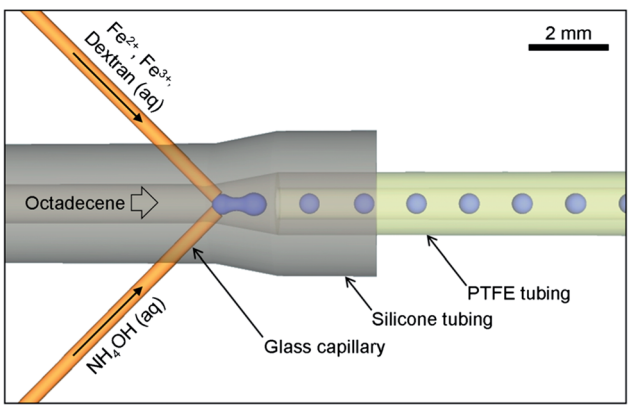

Fig. 1 Schematic of the capillary-based droplet reactor showing the injection of separate precursor streams of Fe^{2+}/Fe^{3+}/dextran and NH_4OH into a continuous stream of octadecene carrier fluid; iron oxide nanoparticles are formed inside the droplets.

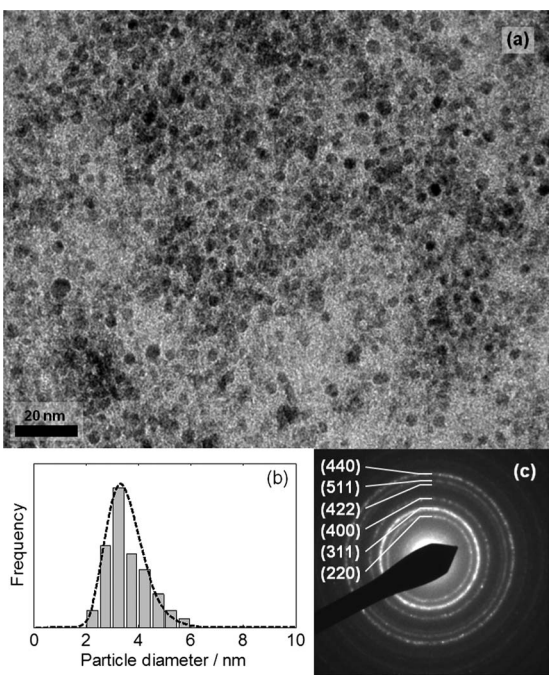

Fig. 2 (a) Transmission electron micrograph of the droplet-synthesised dextran-coated iron oxide nanoparticles. (b) Histogram of particle size obtained from the TEM image; dotted line denotes a log-normal fit. (c) Selected Area Electron Diffraction pattern, with the relevant spinel crystalline planes indicated.

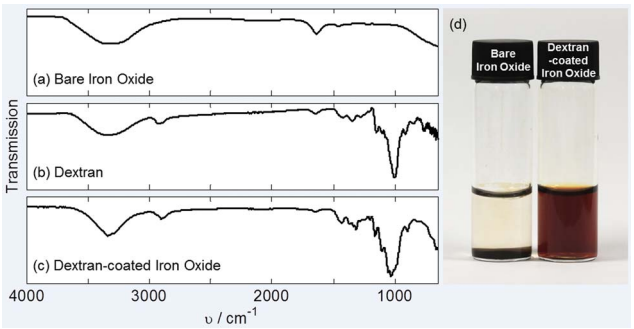

Fig. 3 Solid-state FT-IR spectra of (a) droplet-synthesised uncoated iron oxide; (b) dextran; and (c) droplet-synthesised dextran-coated iron oxide. (d) Photographs of bare and dextran-coated nanoparticle solutions after storage for three weeks.

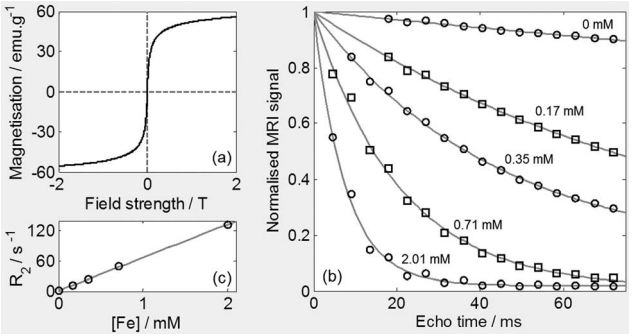

Fig. 4 (a) Room temperature hysteresis traces of superparamagnetic iron oxide nanoparticles obtained by vibrating sample magnetometry. (b) Signal intensity *versus* echo time for particles synthesised in the droplet reactor. (c) Relaxation rate *versus* Fe concentration for particles synthesised in the droplet reactor (relaxivity of 66 $mM^{-1}s^{-1}$).

confirming the principal crystalline product to be spinel phase iron oxide with minimal contamination from other crystalline side products.

Fig. 3 shows solid-state Fourier Transform Infrared (FTIR) spectra for (a) dextran-free iron oxide nanoparticles, (b) dextran and (c) dextran-coated iron oxide nanoparticles. The dextran-free nanoparticles exhibited a relatively simple IR spectrum, with absorption peaks at 3300 and 1600 cm^{-1} due to the OH-stretching and HOH-bending modes of residual water on the particle surface. (Note, the response seen at the low-frequency edge of the spectrum is due to a broad grouping of Fe–O vibrations located between 400 and 600 cm^{-1}).[21] The dextran-only sample exhibited a fairly complex spectrum: in addition to water-related signals at 3300 and 1600 cm^{-1}, a C–H stretching mode was evident at 2900 cm^{-1} plus a cluster of additional features in the "fingerprint" region below 1500 cm^{-1}, including a strong C–O response at 1000 cm^{-1}. The FTIR spectrum of the dextran-coated iron oxide nanoparticles also exhibited the dextran signature, but with a slight broadening and shift of the C–O stretch (and of nearby features in the fingerprint region), consistent with co-ordination of the dextran to the particle surface.[21a]§ The effectiveness of the dextran coating in stabilising the nanoparticles is clear from Fig. 3d which shows coated and non-coated particles after storage for three weeks: the uncoated particles aggregated and settled to the bottom of the vial whereas the dextran-coated samples remained fully dispersed as a clear red-brown solution.

The as-produced iron oxide nanoparticles are attractive candidates for *in vivo* imaging applications due to their small size, narrow size distributions, and biocompatible dextran surface-coating. To assess their potential as MRI T_2 contrast enhancement agents, the magnetic properties of the particles were first characterised using vibrating sample magnetometry (VSM). The particles yielded a magnetisation curve with zero remanence and coercivity (see Fig. 4a), indicating the sample to be superparamagnetic with minimal contamination from non-superparamagnetic species such as α-Fe_2O_3 (hematite). The saturation magnetisation was 58 emu/g, which compares favourably to typical values of 30–50 emu/g reported elsewhere in the literature for SPIONs obtained by co-precipitation.[22]

For the MRI measurements, solutions of the droplet-synthesised SPIONs were prepared at varying concentrations from 0 (reference) to 2.0 mM Fe, and measurements were made in the T_2 (spin–spin) relaxation mode using a 4.7 T MRI spectrometer (see Experimental). Fig. 4b shows the normalised MRI signal S *versus* time t for the various SPION concentrations, with the markers corresponding to experimental data and the solid lines denoting numerical fits to exponential decay curves of the form $S = \exp(-t/T_2)$. Plotting the relaxation rate constant ($R_2 = 1/T_2$) against Fe concentration (Fig. 4c) yielded a straight line[21] of slope 66 ± 1 $mM^{-1}s^{-1}$, corresponding to the r_2 relaxivity of the as-produced particles. This value compares favourably with r_2 relaxivities of 62 $mM^{-1}s^{-1}$ and 110 $mM^{-1}s^{-1}$ reported for cross-linked iron oxide (CLIO) nanoparticles and Feridex™; at 4.5 T,[23] and confirms the viability of the droplet-synthesised SPIONs as MRI contrast agents.

Conclusions

In conclusion, we report the use of a stable passively driven capillary-based droplet reactor for the aqueous preparation of dextran-coated superparamagnetic iron oxide nanoparticles. The reactor yielded small, stable, highly crystalline particles with a narrow size distribution (σ_d/d = 22%), a large saturation magnetisation of 58 emu/g, and a high T_2 relaxivity of 66 $mM^{-1}s^{-1}$. The scalable nature of the microfluidic synthesis route combined with the narrow size distribution and high T_2 relaxivities of the resultant particles offers a promising route to the controlled synthesis of superparamagnetic iron-oxide nanoparticles that overcomes many of the limitations of conventional (batch) co-precipitation methods.

Experimental

Device fabrication

Two incisions were made on opposite sides of a 10 cm length of silicone tubing (VWR, ID 1 mm, OD 3 mm), approximately 2 cm from the end. Into the incisions were inserted two glass capillaries of length ~5 cm (Polymicro, ID 150 μm, OD 375 μm), making an

§ Note, in the case of larger particles of diameter greater than about 15 nm (synthesized in the capillary reactor under different reaction conditions), Transmission Electron Micrographs clearly show the presence of a ~3 nm shell surrounding each iron-oxide core, see ESI. For smaller particles, however, the shell cannot be distinguished from the core due to insufficient image contrast.

angle of 90° to each other. A 4.5 m length of PTFE tubing (VWR, ID 0.82 mm) was inserted into the end of the silicone tubing and forced inwards until the PTFE tubing was within 1.5 mm of the capillary tips. 4 m of the central section of the PTFE tubing was coiled to permit insertion into an oil bath.

Sample preparation and purification

Precursor solutions of dextran, ferrous chloride tetrahydrate (Sigma Aldrich, UK), ferric chloride hexahydrate (Sigma Aldrich, UK), and ammonium hydroxide (Sigma Aldrich, UK) were loaded into separate 10 ml syringes (BD, Plastipak, UK). The syringes were connected to fluorinated ethylene propylene (FEP) tubing (Upchurch Scientific, 356 μm i.d., 1.57 mm o.d.) using polyether ether ketone Luer-lock interconnects (Upchurch Scientific). The FEP tubing was then connected directly to the glass auxiliary capillaries of the droplet reactor. Octadecene (ODE) carrier fluid was loaded into a 50 ml syringe fitted with a Luer-lock dispensing tip (Intertronics, 1.5 mm o.d.) which was inserted into the vacant end of the silicone tubing.

Following particle synthesis (described in the main text), the nanoparticles were purified by separating the aqueous phase from the organic carrier fluid using a pipette and then centrifuging at 4500 rpm for 15 min to yield a brown solid of iron oxide and supernatant containing unused reactants. The supernatant was removed, and the solid re-dissolved in de-ionised water. The centrifugation/redissolution procedure was repeated several times.

Transmission electron microscopy

The HRTEM images and SAED pattern were obtained with a JEOL 2010 Electron Microscope (JEOL, Tokyo, Japan) operating at 200 KeV. A drop of the prepared sample was placed on a carbon covered copper grid (Agar Scientific, UK) and left to dry for one hour and then imaged under the electron microscope.

Vibrating sample magnetometry

After drying a concentrated solution of the iron oxide nanoparticles under vacuum overnight, a 2.7 ± 0.2 mg sample was taken, placed on a 2 mm × 2 mm filter paper, and mounted on the VSM sample holder. Magnetization of the nanoparticles was measured as a function of applied field in four quadrant MH loops using an Oxford Instruments VSM equipped with a 5T transverse split-coil magnet.

Magnetic resonance imaging

MRI was performed using a 4.7 T Magnex magnet (Oxford, UK) and a Varian Unity Inova console (Palo Alto, CA, USA). All samples were diluted in HEPES buffer (0.01 M, pH 7.0) to obtain eight samples with varying iron concentrations in the range 0–0.169 mg mL^{-1}. Iron concentrations were determined using Inductively Coupled Plasma-Atomic Emission Spectroscopy (ICP-AES) (Vista-Pro Axial, Varian). Samples were then added to Eppendorf tubes (200 μL) and placed in a quadrature ^{1}H coil. All measurements were made at room temperature. T_2 values were obtained using a saturation recovery experiment[24] performed with a standard spin-echo sequence and a single slice acquisition (TR = 3000 ms, TE values = 4.5, 9.0, 13.5, 18.0, 22.5, 27.0, 31.5, 36.0, 40.5, 45.0, 49.5, 54.0, 58.5, 63.0, 67.5 and 72 ms, slice thickness: 9 mm, number of signal averages: 10, FOV: 100 × 50 mm^2).

Acknowledgements

We acknowledge funding from the EPSRC through the Knowledge Transfer Secondment Scheme, the Royal Society under its Industry Fellowship scheme, and the EC Seventh Framework programme (FP7/2007–2013) under grant agreement number CP-FP 214478-2.

References

1 J. Dobson, Magnetic nanoparticles for drug delivery, *Drug Dev. Res.*, 2006, **67**(1), 55–60.
2 S. Laurent, S. Dutz, U. O. Haefeli and M. Mahmoudi, Magnetic fluid hyperthermia: Focus on superparamagnetic iron oxide nanoparticles, *Adv. Colloid Interface Sci.*, 2011, **166**(1–2), 8–23.
3 (*a*) D. Pouliquen, H. Perroud, F. Calza, P. Jallet and J. J. Lejeune, Investigation of the magnetic-properties of iron-oxide nanoparticles used as contrast agent for MRI, *Magn. Reson. Med.*, 1992, **24**(1), 75–84; (*b*) Y. X. J. Wang, S. M. Hussain and G. P. Krestin, Superparamagnetic iron oxide contrast agents: physicochemical characteristics and applications in MR imaging, *Eur. Radiol.*, 2001, **11**(11), 2319–2331.
4 M. V. Kutushov; A. A. Kuznetsov; V. I. Filippov; O. A. Kuznetsov, *New method of biological fluid detoxification based on magnetic adsorbents*. Plenum Press Div Plenum Publishing Corp: New York, 1997; p 391–397.
5 J. B. Edel, R. Fortt, J. C. deMello and A. J. deMello, Microfluidic routes to the controlled production of nanoparticles, *Chem. Commun.*, 2002, 1136–1137.
6 (*a*) D. V. R. Kumar, M. Kasture, A. A. Prabhune, C. V. Ramana, B. L. V. Prasad and A. A. Kulkarni, Continuous flow synthesis of functionalized silver nanoparticles using bifunctional biosurfactants, *Green Chem.*, 2010, **12**(4), 609–615; (*b*) L. L. Lazarus, A. S. J. Yang, S. Chu, R. L. Brutchey and N. Malmstadt, Flow-focused synthesis of monodisperse gold nanoparticles using ionic liquids on a microfluidic platform, *Lab Chip*, 2010, **10**(24), 3377–3379; (*c*) S. Duraiswamy and S. A. Khan, Droplet-Based Microfluidic Synthesis of Anisotropic Metal Nanocrystals, *Small*, 2009, **5**(24), 2828–2834; (*d*) C. H. H. Weng, C. C. Yeh, C. S. Lee, G. B. Ieee, *Synthesis of Gold Nanoparticles Using Microfluidic Reaction Systems*. IEEE: New York, 2007; p 464–468; (*e*) Y. J. Song, P. Y. Jin and T. Zhang, Microfluidic synthesis of Fe nanoparticles, *Mater. Lett.*, 2010, **64**(16), 1789–1792.
7 (*a*) A. Abou Hassan, O. Sandre, V. Cabuil and P. Tabeling, Synthesis of iron oxide nanoparticles in a microfluidic device: preliminary results in a coaxial flow millichannel, *Chem. Commun.*, 2008, 1783–1785; (*b*) B. F. Cottam, S. Krishnadasan, A. J. deMello, J. C. deMello and M. S. P. Shaffer, Accelerated synthesis of titanium oxide nanostructures using microfluidic chips, *Lab Chip*, 2007, **7**(2), 167–169; (*c*) L. Frenz, A. El Harrak, M. Pauly, S. Begin-Colin, A. D. Griffiths and J. C. Baret, Droplet-based microreactors for the synthesis of magnetic iron oxide nanoparticles, *Angew. Chem., Int. Ed.*, 2008, **47**(36), 6817–6820; (*d*) M. Takagi, T. Maki, M. Miyahara and K. Mae, Production of titania nanoparticles by using a new microreactor assembled with same axle dual pipe, *Chem. Eng. J.*, 2004, **101**(1–3), 269–276.
8 (*a*) S. Krishnadasan, R. J. C. Brown, A. J. deMello and J. C. deMello, Intelligent routes to the controlled synthesis of nanoparticles, *Lab Chip*, 2007, **7**(11), 1434–1441; (*b*) A. M. Nightingale and J. C. de Mello, Controlled Synthesis of III–V Quantum Dots in Microfluidic Reactors, *ChemPhysChem*, 2009, **10**(15), 2612–2614; (*c*) B. K. H. Yen, N. E. Stott, K. F. Jensen and M. G. Bawendi, A continuous-flow microcapillary reactor for the preparation of a size series of CdSe nanocrystals, *Adv. Mater.*, 2003, **15**(21), 1858–1862.
9 J. Puigmarti-Luis, D. Schaffhauser, B. R. Burg and P. S. Dittrich, A Microfluidic Approach for the Formation of Conductive

Nanowires and Hollow Hybrid Structures, *Adv. Mater.*, 2010, **22**(20), 2255.
10 (*a*) A. J. deMello, Control and detection of chemical reactions in microfluidic systems, *Nature*, 2006, **442**(7101), 394–402; (*b*) C.-X. Zhao, L. He, S. Z. Qiao and A. P. J. Middelberg, Nanoparticle synthesis in microreactors, *Chem. Eng. Sci.*, 2011, **66**(7), 1463–1479; (*c*) A. M. Nightingale and J. C. de Mello, Microscale synthesis of quantum dots, *J. Mater. Chem.*, 2010, **20**(39), 8454–8463; (*d*) J. DeMello and A. DeMello, Microscale reactors: nanoscale products, *Lab Chip*, 2004, **4**(2), 11N–15N.
11 E. M. Chan, A. P. Alivisatos and R. A. Mathies, High-temperature microfluidic synthesis of CdSe nanocrystals in nanoliter droplets, *J. Am. Chem. Soc.*, 2005, **127**(40), 13854–13861.
12 A. M. Nightingale, S. H. Krishnadasan, D. Berhanu, X. Niu, C. Drury, R. McIntyre, E. Valsami-Jones and J. C. deMello, A stable droplet reactor for high temperature nanocrystal synthesis, *Lab Chip*, 2011, **11**(7), 1221–1227.
13 H. Song, J. D. Tice and R. F. Ismagilov, A microfluidic system for controlling reaction networks in time, *Angew. Chem., Int. Ed.*, 2003, **42**(7), 768–772.
14 W.-B. Lee, C.-H. Weng, F.-Y. Cheng, C.-S. Yeh, H.-Y. Lei and G.-B. Lee, Biomedical microdevices synthesis of iron oxide nanoparticles using a microfluidic system, *Biomed. Microdevices*, 2009, **11**(1), 161–171.
15 D. L. J. Thorek, A. Chen, J. Czupryna and A. Tsourkas, Superparamagnetic iron oxide nanoparticle probes for molecular imaging, *Ann. Biomed. Eng.*, 2006, **34**(1), 23–38.
16 R. Massart, Preparation of aqueous magnetic liquids in alkaline and acidic media, *IEEE Trans. Magn.*, 1981, **17**(2), 1247–1248.
17 F. Q. Yu and V. C. Yang, Size-tunable synthesis of stable superparamagnetic iron oxide nanoparticles for potential biomedical applications, *J. Biomed. Mater. Res. Part A*, 2010, **92A**(4), 1468–1475.
18 S. Laurent, D. Forge, M. Port, A. Roch, C. Robic, L. V. Elst and R. N. Muller, Magnetic iron oxide nanoparticles: Synthesis, stabilization, vectorization, physicochemical characterizations, and biological applications, *Chem. Rev.*, 2008, **108**(6), 2064–2110.
19 N. M. Gribanov, E. E. Bibik, O. V. Buzunov and V. N. Naumov, Physico-chemical regularities of obtaining highly dispersed magnetite by the method of chemical condensation, *J. Magn. Magn. Mater.*, 1990, **85**(1–3), 7–10.
20 S. Asuha, B. Suyala, X. Siqintana and S. Zhao, Direct synthesis of Fe3O4 nanopowder by thermal decomposition of Fe-urea complex and its properties, *J. Alloys Compd.*, 2011, **509**(6), 2870–2873.
21 (*a*) D. Predoi, E. Andronescu, M. Radu, M. C. Munteanu and A. Dinischiotu, Synthesis and characterization of bio-compatible maghemite nanoparticles, *Dig. J. Nanomater. Biostruct.*, 2010, **5**(3), 779–786; (*b*) D. Predoi, A study on iron oxide nanoparticles coated with dextrin obtained by coprecipitation, *Digest Journal of Nanomaterials and Biostructures*, 2007, **2**(1), 169–173; (*c*) G. Liu, R. Y. Hong, L. Guo, Y. G. Li and H. Z. Li, Preparation, characterization and MRI application of carboxymethyl dextran coated magnetic nanoparticles, *Appl. Surf. Sci.*, 2011, **257**(15), 6711–6717.
22 A.-H. Lu, E. L. Salabas and F. Schueth, Magnetic nanoparticles: Synthesis, protection, functionalization, and application, *Angew. Chem., Int. Ed.*, 2007, **46**(8), 1222–1244.
23 J.-t. Jang, H. Nah, J.-H. Lee, S. H. Moon, M. G. Kim and J. Cheon, Critical Enhancements of MRI Contrast and Hyperthermic Effects by Dopant-Controlled Magnetic Nanoparticles, *Angew. Chem., Int. Ed.*, 2009, **48**(7), 1234–1238.
24 G. A. Morris and A. J. Freemont, Direct observation of the magnetization exchange dynamics responsible for magnetization transfer contrast in human cartilage *in vitro*, *Magn. Reson. Med.*, 1992, **28**(1), 97–104.

